

NAT'L INST. OF STAND & TECH



A11106 323391

NIST
PUBLICATIONS

REFERENCE

NISTIR 6892

The Effect of Anisotropic Surface Energy on the Rayleigh Instability

***K. F. Gurski
G. B. McFadden***

U. S. DEPARTMENT OF COMMERCE
Technology Administration
National Institute of Standards
and Technology
Gaithersburg, MD 20899

QC
100
.456
#6892
2002

NIST

**National Institute of Standards
and Technology**
Technology Administration
U.S. Department of Commerce

The Effect of Anisotropic Surface Energy on the Rayleigh Instability

K. F. Gurski
G. B. McFadden

U. S. DEPARTMENT OF COMMERCE
Technology Administration
National Institute of Standards
and Technology
Gaithersburg, MD 20899

November 2002



U.S. DEPARTMENT OF COMMERCE
Donald L. Evans, Secretary
TECHNOLOGY ADMINISTRATION
Phillip J. Bond, Under Secretary for Technology
NATIONAL INSTITUTE OF STANDARDS
AND TECHNOLOGY
Arden L. Bement, Jr., Director

The Effect of Anisotropic Surface Energy on the Rayleigh Instability

BY K. F. GURSKI AND G. B. MCFADDEN

*National Institute of Standards and Technology, Gaithersburg, MD 20899-8910,
USA*

We determine the linear stability of a rod or wire subject to capillary forces arising from an anisotropic surface energy. The rod is assumed to be smooth with an uniform cross section given by a 2-D equilibrium shape. The stability analysis is based on computing the sign of the second variation of the total energy, which is examined by solving an associated eigenvalue problem. The eigenproblem is a coupled pair of second-order ordinary differential equations with periodic coefficients that depend on the second derivatives of the surface energy with respect to orientation variables. We apply the analysis to examples with uniaxial or cubic anisotropy, which illustrate that anisotropic surface energy plays a significant role in establishing the stability of the rod. Both the magnitude and sign of the anisotropy determine whether the contribution stabilizes or destabilizes the system relative to the case of isotropic surface energy, which reproduces the classical Rayleigh instability.

Keywords: Rayleigh instability, anisotropic surface energy, quantum wires, nanorods, Cahn-Hoffman xi-vector

1. Introduction

As shown by Plateau (1873) in his classical studies of capillary instabilities, a cylindrical interface with an isotropic surface free energy is unstable to volume-preserving axisymmetric perturbations whose wavelength exceeds the circumference of the cylinder. Such perturbations lower the total energy of the cylinder, leading to the breakup of the cylinder into a series of drops or bubbles. The stability of a liquid jet was subsequently studied by Lord Rayleigh (1878), who argued that the length scale of the instability is determined by the perturbations having the fastest temporal growth rate of instability; the phenomenon has generally come to be known as the Rayleigh instability.

The Rayleigh instability arises in a number of diverse applications, such as ink jet printing (Pimbley & Lee 1977), two-phase flow (Taylor 1934; Tomotika 1936), liquid bridges (Coriell *et al.* 1977; Zhang & Alexander 1990; Slobozhanin *et al.* 1997; Lowry & Steen 1997), quantum wires (Fukunaga *et al.* 1998; Kassubek *et al.* 2001), fiber spinning (Hohman *et al.* 2001), liquid crystals (Forest & Wang 1998), and polymer blends (Migler 2001). In solidification, a cylindrical interface is subject to capillary instabilities (Marinis & Sekerka 1979; Brattkus 1989; McFadden *et al.* 1993; Majumdar & Chattopadhyay 1996). A crystal-melt interface in an isothermal system is subject to a Rayleigh instability through the Gibbs-Thomson equation,

but the system can be stabilized by radial temperature gradients normal to the interface (McFadden *et al.* 1993).

Because of the underlying crystal lattice, the surface energy of a liquid-solid or vapor-solid interface is generally anisotropic and depends on the orientation of the local normal vector at each point of the interface (Herring 1953; Mullins 1963; Rottman & Wortis 1984). The surface energy of a solid-solid interface between two crystals is also anisotropic in general, with the additional complication that the surface energy also depends on the direction cosines that characterize the relative orientations of the two crystals (Sutton & Balluffi 1995). For the case that the two crystals share a common lattice orientation, as in an anti-phase boundary, the solid-solid surface energy can also be assumed to depend on the local normal vector. In this paper we will consider a model of this type in which the surface energy depends only on the local normal vector.

An observation that partially motivates this work is the apparent stability of elongated nanowires that are grown in a bridge configuration (e.g., Kondo & Takayanagi 1997) or epitaxially on a heterogeneous substrate (e.g., Chen *et al.* 2000, 2001). The nanowires (alternatively called nanorods or quantum wires) are “one-dimensional” crystals with dimensions as small as one nanometer high, a few nanometers wide, and can be as long as a micron. There are long-standing studies on possible experimental techniques to grow these nanowires (Sundaram *et al.* 1991), and the stability of these nanowires is beginning to come under study. Continuum modeling of the nanowires provides some guidance as to their expected stability, though the strict applicability of continuum models is limited if the length scales approach atomic dimensions. There are a number of possible mechanisms that could stabilize the wire, including elastic interactions between the wire and the substrate (Chen *et al.* 2000), quantum electronic shell effects (Kassubek *et al.* 2001), and surface energy anisotropy (Loretto *et al.* 1996).

A linear stability analysis suggests that isolated quantum wires with an isotropic surface energy would tend to bead up rather than persist as wires. Numerous studies of similar structures have shown that the Rayleigh instability leads preferentially to the formation of droplets or particles (Fukunaga *et al.* 1998; Forest & Wang 1998; Majumdar & Chattopadhyay 1996). Recently Kassubek *et al.* (2001) performed a linear stability analysis of nanowires with a free-electron model using quantum chaos techniques. They found that the instability of a long wire under isotropic surface tension can be completely suppressed by electronic shell effects.

To address the effects of surface tension anisotropy on the Rayleigh instability, we compute the second variation of the surface free energy of an isolated wire or rod whose cross section is smooth and given by the associated two-dimensional equilibrium shape. Previously Cahn (1979) studied the stability of rods with circular cross-sections that are subject to axisymmetric perturbations; the underlying surface free energy is assumed to have transverse isotropy, which results in closed-form solutions to the stability problem. In our study, we consider general surface free energies and derive an associated eigenproblem whose eigenvalues govern the stability of the rod. The eigenproblem is described by a pair of coupled second-order ordinary differential equations with periodic coefficients, which generally lack closed-form solutions. We apply the analysis to a number of examples, including the case of a cubic material, and compute the stability of the rod to general perturbations when the axis of the rod is in high symmetry orientations such as [001],

[011], and [111]. For small levels of anisotropy, the stability can be computed approximately via perturbation theory. For larger amplitudes of anisotropy, we have computed solutions numerically. We find that surface tension anisotropy can either promote or suppress the Rayleigh instability, depending on the orientation of the wire and the magnitude and sign of the anisotropy.

2. Model

We compute the stability of an infinite rod extending in the z direction of a cartesian coordinate system (x, y, z) . The cross section of the rod is assumed to be uniform in z and defined by a two-dimensional (2-D) equilibrium shape which is determined by surface energy considerations alone. We assume that the surface energy is anisotropic, depending on the orientation of the local normal to the surface, but restrict our attention to differentiable surface energies with anisotropies that are mild enough that the surface of the rod is smooth and does not exhibit any missing orientations.

(a) 2-D Cross Section

Under these assumptions the cross section of the rod in the (x, y) plane can then be written in the parametric form (see, e.g., Voorhees *et al.* 1984)

$$X(\phi) = \frac{\ell}{\gamma_0} [\bar{\gamma}(\phi) \cos \phi - \bar{\gamma}_\phi(\phi) \sin \phi], \quad Y(\phi) = \frac{\ell}{\gamma_0} [\bar{\gamma}(\phi) \sin \phi + \bar{\gamma}_\phi(\phi) \cos \phi], \quad (2.1)$$

for $0 \leq \phi \leq 2\pi$, where $\bar{\gamma}(\phi)$ is the 2-D surface energy, ℓ is a characteristic length scale, and γ_0 is a characteristic surface energy. Here derivatives are denoted by subscripts, with $\bar{\gamma}_\phi = d\bar{\gamma}/d\phi$. The relation of the 2-D surface energy $\bar{\gamma}(\phi)$ to the more general 3-D surface energy that characterizes a given material will be discussed shortly.

The curve defined by eq. (2.1) has the outward normal $\hat{r}(\phi) = (\cos \phi, \sin \phi)$, so the shape is parameterized in terms of its normal angle ϕ ; see figure 5. The angle ϕ is also the appropriate argument for the surface energy $\bar{\gamma} = \bar{\gamma}(\phi)$. In addition, the curvature of the shape, $\mathcal{K} = (X_\phi Y_{\phi\phi} - Y_\phi X_{\phi\phi})/[X_\phi^2 + Y_\phi^2]^{3/2}$, is found to satisfy a version of the anisotropic Gibbs-Thomson equation,

$$[\bar{\gamma} + \bar{\gamma}_{\phi\phi}] \mathcal{K} = \frac{\gamma_0}{\ell}. \quad (2.2)$$

A 2-D equilibrium shape is therefore characterized by a constant weighted mean curvature $[\bar{\gamma} + \bar{\gamma}_{\phi\phi}] \mathcal{K}$ (Taylor 1992). For an isotropic surface energy $\bar{\gamma}(\phi) = \gamma_0$, the 2-D equilibrium shape (2.1) reduces to a circle of radius ℓ . Missing orientations occur if $\bar{\gamma} + \bar{\gamma}_{\phi\phi} < 0$ (Voorhees *et al.* 1984); we will assume $\bar{\gamma} + \bar{\gamma}_{\phi\phi} > 0$.

(b) Shape Perturbation

We express the surface of the rod in the dimensionless form

$$\vec{X}^{(0)}(\phi, z) = \bar{\gamma}(\phi) \hat{r}(\phi) + \bar{\gamma}_\phi(\phi) \hat{\phi}(\phi) + z \hat{z}, \quad (2.3)$$

for $0 \leq \phi \leq 2\pi$ and $-\infty < z < \infty$, where $\hat{r}(\phi) = \cos \phi \hat{x} + \sin \phi \hat{y}$, $\hat{\phi}(\phi) = -\sin \phi \hat{x} + \cos \phi \hat{y}$, and \hat{z} are unit vectors in a cylindrical coordinate system. Here the units of

length and energy are based on ℓ and γ_0 , respectively; appropriate choices for ℓ and γ_0 will be described in the examples discussed in §3.

We determine the stability of the rod by computing the total energy of a volume-preserving perturbation to the rod having the general form

$$\vec{X}(\phi, z) = \vec{X}^{(0)}(\phi, z) + \epsilon h(\phi, z) \hat{r}(\phi) + \frac{\epsilon^2}{2} h_2 \hat{r}(\phi) + O(\epsilon^3), \quad (2.4)$$

where ϵ is a small parameter, $h(\phi, z)$ is the height of the perturbation along the normal \hat{r} to the unperturbed shape, and the constant h_2 is a second-order shape correction introduced to satisfy the volume constraint at $O(\epsilon^2)$. The geometry of the perturbed rod is determined by the two tangent vectors \vec{X}_ϕ and \vec{X}_z , and their cross product, $\vec{P} = \vec{X}_\phi \times \vec{X}_z$, which is normal to the interface. The area element on the interface is given by $dA = |\vec{X}_\phi \times \vec{X}_z| d\phi dz = |\vec{P}| d\phi dz$. Evaluating the tangent vectors by using eq. (2.4) and taking their cross product, we find that the interface normal has the expansion

$$\vec{P}(\phi, z) = \vec{P}^{(0)}(\phi, z) + \epsilon \vec{P}^{(1)}(\phi, z) + \frac{\epsilon^2}{2} \vec{P}^{(2)}(\phi, z) + O(\epsilon^3), \quad (2.5)$$

where

$$\vec{P}^{(0)} = (\bar{\gamma} + \bar{\gamma}_{\phi\phi}) \hat{r}, \quad (2.6)$$

$$\vec{P}^{(1)} = h \hat{r} - h_\phi \hat{\phi} - (\bar{\gamma} + \bar{\gamma}_{\phi\phi}) h_z \hat{z}, \quad (2.7)$$

$$\vec{P}^{(2)} = h_2 \hat{r} - 2hh_z \hat{z}. \quad (2.8)$$

The stability of the rod is determined by expanding the total energy through $O(\epsilon^2)$ for $|\epsilon| \ll 1$, and examining whether the shape perturbation raises or lowers the energy of the rod. Since the rod is assumed to be infinite in the z -direction, an analysis in terms of Fourier components allows us to consider shape perturbations that are periodic in z .

(c) Volume Constraint

The shape perturbation is required to preserve the rod's volume over a given length, which we may take to be a period λ of the perturbation. The volume is given by

$$V = \frac{1}{2} \iiint \nabla \cdot (x, y, 0) dV = \frac{1}{2} \int_0^\lambda \int_0^{2\pi} \vec{P}(\phi, z) \cdot [\vec{X}(\phi, z) - z \hat{z}] d\phi dz. \quad (2.9)$$

Expanding in ϵ , we find that

$$V = V^{(0)} + \epsilon V^{(1)} + \frac{\epsilon^2}{2} V^{(2)} + O(\epsilon^3), \quad (2.10)$$

where

$$V^{(0)} = \frac{\lambda}{2} \int_0^{2\pi} \bar{\gamma} (\bar{\gamma} + \bar{\gamma}_{\phi\phi}) d\phi, \quad (2.11)$$

$$V^{(1)} = \int_0^\lambda \int_0^{2\pi} (\bar{\gamma} + \bar{\gamma}_{\phi\phi}) h(\phi, z) d\phi dz, \quad (2.12)$$

$$V^{(2)} = \int_0^\lambda \int_0^{2\pi} \{ [h(\phi, z)]^2 + h_2 \bar{\gamma}(\phi) \} d\phi dz. \quad (2.13)$$

A periodic perturbation $h(\phi, z)$ with mean zero makes $V^{(1)} = 0$, and an appropriate choice of h_2 then enforces $V^{(2)} = 0$, viz.,

$$\lambda h_2 \int_0^{2\pi} \bar{\gamma}(\phi) d\phi = - \int_0^{2\pi} \int_0^\lambda [h(\phi, z)]^2 d\phi dz. \quad (2.14)$$

(d) 3-D Surface Energy

An arbitrary perturbation $h(\phi, z)$ results in orientations on the perturbed shape that do not occur on the original rod, so that knowledge of the 2-D surface energy $\bar{\gamma}(\phi)$ is not enough to determine the stability of the rod: we need to consider the 3-D surface energy for general orientations. We will assume the rod axis is aligned in an arbitrary crystallographic direction. The surface energy of the perturbed rod will be expressed in terms of the interface normal vector written in a spherical coordinate system (ρ, θ, ϕ) in which z is the polar axis, $\rho = \sqrt{x^2 + y^2 + z^2}$ is the 3-D radius, θ is the polar angle, and ϕ is the azimuthal angle; note that ϕ is common to both the cylindrical and spherical coordinate systems (see figure 2). A general interface normal then has components $n_x = \cos \phi \sin \theta$, $n_y = \sin \phi \sin \theta$, and $n_z = \cos \theta$, and the 3-D surface energy can be written as $\gamma = \gamma(\phi, \theta)$. The normal to the unperturbed rod lies in the plane $\theta = \pi/2$, or $n_z = 0$. In this plane the spherical and cylindrical coordinate systems are related by $\hat{\rho} = \hat{r}$ and $\hat{\theta} = -\hat{z}$, and the 2-D surface energy is given by $\bar{\gamma}(\phi) = \gamma(\phi, \pi/2)$.

(i) Cahn-Hoffman ξ -Vector

The calculations are simplified considerably by introducing the ξ -vector formalism developed by Cahn & Hoffmann (1972, 1974). The 3-D ξ -vector is given by (Voorhees *et al.* 1984)

$$\vec{\xi}(\phi, \theta) = \nabla [\rho \gamma(\phi, \theta)] = \gamma \hat{\rho} + \frac{1}{\sin \theta} \gamma_\phi \hat{\phi} + \gamma_\theta \hat{\theta}. \quad (2.15)$$

The dimensionless 3-D equilibrium shape is given by $\vec{\xi}(\phi, \theta)$ for $0 \leq \phi \leq 2\pi$ and $0 \leq \theta \leq \pi$, and its normal is $\hat{\rho}(\phi, \theta)$.

In the plane $\theta = \pi/2$, the ξ -vector traces out the curve

$$\vec{\xi}(\phi, \pi/2) = \gamma \hat{r} + \gamma_\phi \hat{\phi} - \gamma_\theta \hat{z}. \quad (2.16)$$

If $\gamma_\theta(\phi, \pi/2) = 0$ for $0 \leq \phi \leq 2\pi$, this curve lies in the plane $z = 0$ and represents a 2-D equilibrium shape corresponding to the 2-D surface energy $\bar{\gamma}(\phi) = \gamma(\phi, \pi/2)$. If $\gamma_\theta(\phi, \pi/2) \neq 0$, this curve is not confined to the plane $z = 0$. However, the cross section of the rod that is formed by projecting this curve to the plane $z = 0$ is the 2-D equilibrium shape corresponding to $\bar{\gamma}(\phi)$. The rods that we consider here are related to the 3-D surface energy $\gamma(\phi, \theta)$ in this manner.

More generally, we can define the ξ -vector on an arbitrary surface $\vec{X}(u, v)$ with a normal vector field $\vec{P} = \vec{X}_u \times \vec{X}_v$ as follows. We first extend the definition of $\gamma(\phi, \theta)$ by writing

$$\Gamma(\vec{P}) = |\vec{P}| \gamma(\Theta, \Phi), \quad (2.17)$$

where

$$\Theta = \tan^{-1}(\sqrt{P_x^2 + P_y^2}/P_z), \quad \Phi = \tan^{-1}(P_y/P_x), \quad (2.18)$$

are the corresponding spherical angles based on the normal vector \vec{P} . Since we have

$$\gamma(\Theta, \Phi) dA = \gamma(\Theta, \Phi) |\vec{P}| du dv = \Gamma(\vec{P}) du dv, \quad (2.19)$$

the total energy of the shape has the simple form

$$E = \iint \Gamma(\vec{P}) du dv. \quad (2.20)$$

Variations in E due to changes in the surface shape then lead directly to the Cahn-Hoffman ξ -vector, with components

$$\xi_j(\vec{P}) = \frac{\partial \Gamma(\vec{P})}{\partial P_j}. \quad (2.21)$$

The 3-D weighted mean curvature of the surface associated with $\gamma(\Phi, \Theta)$ is then given by the surface divergence of the ξ -vector, $\nabla_S \cdot \vec{\xi}$ (Taylor 1992).

For our system, the surface and normal vectors are given by eq. (2.4) and eq. (2.5), respectively, and the energy, E , of the shape over a single period is

$$E = \int_0^\lambda \int_0^{2\pi} \Gamma(\vec{P}) d\phi dz. \quad (2.22)$$

By using the definition (2.21) and the relations (2.5), we find the expansion

$$\Gamma(\vec{P}) = \Gamma(\vec{P}^{(0)}) + \epsilon \vec{\xi}^{(0)} \cdot \vec{P}^{(1)} + \frac{\epsilon^2}{2} [\vec{\xi}^{(0)} \cdot \vec{P}^{(2)} + \vec{\xi}^{(1)} \cdot \vec{P}^{(1)}] + O(\epsilon^3), \quad (2.23)$$

where we have

$$\Gamma(\vec{P}^{(0)}) = \gamma(\gamma + \gamma_{\phi\phi}), \quad (2.24)$$

$$\vec{\xi}^{(0)} = \gamma \hat{r} + \gamma_{\phi} \hat{\phi} - \gamma_{\theta} \hat{z}, \quad (2.25)$$

$$\vec{\xi}^{(1)} = [\gamma_{\theta\phi} h_z - h_{\phi}] \hat{\phi} + \left[\frac{\gamma_{\theta\phi} h_{\phi}}{(\gamma + \gamma_{\phi\phi})} - (\gamma + \gamma_{\theta\theta}) h_z \right] \hat{z}. \quad (2.26)$$

These expressions result from calculations which are outlined in Appendix I. In these expressions γ and its derivatives are evaluated for the unperturbed rod with $\theta = \pi/2$.

The formal expansion of the energy in powers of ϵ then yields

$$E = E^{(0)} + \epsilon E^{(1)} + \frac{\epsilon^2}{2} E^{(2)} + O(\epsilon^3), \quad (2.27)$$

where

$$E^{(0)} = \lambda \int_0^{2\pi} \gamma (\gamma + \gamma_{\phi\phi}) d\phi, \quad (2.28)$$

$$E^{(1)} = \int_0^\lambda \int_0^{2\pi} (\gamma + \gamma_{\phi\phi}) h d\phi dz, \quad (2.29)$$

$$E^{(2)} = \int_0^\lambda \int_0^{2\pi} \left\{ (\gamma + \gamma_{\theta\theta}) (\gamma + \gamma_{\phi\phi}) h_z^2 - 2\gamma_{\theta\phi} h_z h_\phi + h_\phi^2 + 2\gamma_{\theta\theta} h h_z + \gamma h_z^2 \right\} d\phi dz. \quad (2.30)$$

In these expressions, the surface energy $\gamma(\phi, \theta)$ and its derivatives are all evaluated at $\theta = \pi/2$, so that the coefficients of $h(\phi, z)$ and its derivatives are all independent of z . For a perturbation that is periodic in z , the terms proportional to h_z and $h h_z$ then integrate to zero. The first variation $E^{(1)}$ therefore vanishes for perturbations with $V^{(1)} = 0$, and the rod is in equilibrium. By substituting the value of h_z from eq. (2.14), we find that the second variation is given by

$$E^{(2)} = \int_0^\lambda \int_0^{2\pi} \left\{ h_\phi^2 + (\gamma + \gamma_{\theta\theta}) (\gamma + \gamma_{\phi\phi}) h_z^2 - h^2 - 2\gamma_{\theta\phi} h_\phi h_z \right\} d\phi dz. \quad (2.31)$$

This expression generalizes the axisymmetric formulation of Cahn (1979), in which both the surface energy and the shape perturbation are independent of ϕ .

(e) Eigenproblem

The sign of $E^{(2)}$ can be determined by diagonalizing the associated quadratic form via normal modes. We first define the (indefinite) inner product of two functions $f(\phi, z)$ and $g(\phi, z)$ to be

$$(f, g) = \int_0^\lambda \int_0^{2\pi} \left\{ f_\phi g_\phi + (\gamma + \gamma_{\theta\theta}) (\gamma + \gamma_{\phi\phi}) f_z g_z - fg - \gamma_{\theta\phi} (f_z g_\phi + f_\phi g_z) \right\} d\phi dz, \quad (2.32)$$

so that $E^{(2)} = (h, h)$. We then integrate by parts to obtain

$$(f, g) = - \int_0^\lambda \int_0^{2\pi} f Lg d\phi dz, \quad (2.33)$$

where the boundary terms vanish by periodicity, and

$$Lg = g_{\phi\phi} + g + (\gamma + \gamma_{\phi\phi})(\gamma + \gamma_{\theta\theta})g_{zz} - \gamma_{\theta\phi}g_{z\phi} - [\gamma_{\theta\phi}g_z]_\phi. \quad (2.34)$$

Since L is symmetric, it has a complete set of orthogonal eigenfunctions $h_n(\phi, z)$ with real eigenvalues μ_n . Expanding the perturbation as

$$h(\phi, z) = \sum_n a_n h_n(\phi, z) \quad (2.35)$$

then leads to

$$E^{(2)} = \left(\sum_m a_m h_m, \sum_n a_n h_n \right) = - \sum_{m,n} a_m a_n \int_0^\lambda \int_0^{2\pi} h_m Lh_n d\phi dz$$

$$= - \sum_n \mu_n a_n^2 \int_0^\lambda \int_0^{2\pi} h_n^2 d\phi dz. \quad (2.36)$$

If $\mu_n < 0$ for all n , then the energy increases for any perturbation and the rod is stable. An unstable mode corresponds to a positive value for μ_n .

Since the eigenproblem

$$Lh_n = \mu_n h_n \quad (2.37)$$

has coefficients that are independent of z , we may separate variables by writing

$$h_n(\phi, z) = H_n(\phi) \sin kz + G_n(\phi) \cos kz, \quad (2.38)$$

where $k = 2\pi/\lambda$ is the axial wavenumber, leading to the coupled equations

$$\frac{d^2 H_n}{d\phi^2} + [1 - k^2(\gamma + \gamma_{\phi\phi})(\gamma + \gamma_{\theta\theta})]H_n - k\gamma_{\theta\phi} \frac{dG_n}{d\phi} - k \frac{d}{d\phi}[\gamma_{\theta\phi} G_n] = \mu_n H_n, \quad (40)$$

$$\frac{d^2 G_n}{d\phi^2} + [1 - k^2(\gamma + \gamma_{\phi\phi})(\gamma + \gamma_{\theta\theta})]G_n + k\gamma_{\theta\phi} \frac{dH_n}{d\phi} + k \frac{d}{d\phi}[\gamma_{\theta\phi} H_n] = \mu_n G_n. \quad (41)$$

If $\gamma_{\theta\phi} = 0$ for $0 \leq \phi \leq 2\pi$ the equations decouple.

A critical wavenumber $k = k_c$ corresponds to a marginally-stable mode with $\mu_n = 0$. Such a mode can also be interpreted as representing the bifurcation of another steady-state solution from the infinite rod. In Appendix II we show that Lh is the linearization of the weighted mean curvature $\nabla_S \cdot \vec{\xi}$, so that our energy analysis is equivalent to a bifurcation analysis of the governing equation $\nabla_S \cdot \vec{\xi} = \text{constant}$.

3. Examples

The linear stability problem has closed form solutions for special surface energies and rod orientations. More generally, the eigenproblem has variable coefficients, but easily can be solved numerically for general energies $\gamma(\theta, \phi)$ as long as there are no missing orientations. For small anisotropies, the eigenproblem can be solved approximately by an asymptotic expansion. In this section we discuss a number of examples to illustrate the stability results.

(a) Isotropic Surface Energy

In the isotropic case, the dimensionless problem is reduced to $\gamma(\phi, \theta) = 1$, and the unperturbed rod is a cylinder of radius unity. The eigenproblem has constant coefficients and decouples; the eigenfunctions $H_n = \cos n\phi$ or $\sin n\phi$ correspond to eigenvalues

$$\mu_n = -n^2 + 1 - k^2. \quad (3.1)$$

The eigenmodes with $n \geq 1$ are all stable, and the axisymmetric mode $n = 0$ is stable for $k > 1$ or $\lambda < 2\pi$. We thus recover Plateau's classical result that

axisymmetric perturbations with wavelengths longer than the circumference of the rod are unstable.

We emphasize that the eigenvalues μ_n do not correspond to temporal growth rates arising in a dynamical theory of stability, as in, *e.g.*, Rayleigh's treatment of liquid jets. Temporal growth rates of cylindrical instabilities are often found to be neutrally stable for zero wavenumber [see Chandrasekhar (1961)], whereas our eigenvalues tend to non-zero limits for small wavenumbers.

(b) Ellipsoidal Surface Energy

We next consider a surface energy Γ of the form

$$\Gamma(\vec{P}) = \sqrt{a_x^2 P_x^2 + a_y^2 P_y^2 + a_z^2 P_z^2}, \quad (3.2)$$

in the notation of eq. (2.17). The components of the ξ -vector then satisfy

$$\frac{\xi_x^2}{a_x^2} + \frac{\xi_y^2}{a_y^2} + \frac{\xi_z^2}{a_z^2} = 1, \quad (3.3)$$

so the corresponding equilibrium shape is ellipsoidal with semimajor axes in the ratio $a_x:a_y:a_z$.

We take $a_x = a_y = 1$, resulting in the axisymmetric equilibrium shape $x^2 + y^2 + z^2/a_z^2 = 1$. For $a_z \gg 1$, the shape approximates the unit cylinder $x^2 + y^2 = 1$ near $z = 0$, and, ignoring the effects of surface energy anisotropy, one might expect to recover a Rayleigh instability for wavenumbers $k < 1$. However, equilibrium shapes represent minimum energy configurations and are stable (Johnson & Chakerian 1965), which must be reflected in the stability results of the infinite cylinder.

The surface energy γ for $a_x = a_y = 1$ is given by $\gamma(\phi, \theta) = \sqrt{\sin^2 \theta + a_z^2 \cos^2 \theta}$, and in the plane $\theta = \pi/2$ we have $\gamma = 1$, $\gamma_{\phi\phi} = 0$, $\gamma_{\theta\theta} = 0$, and $\gamma_{\theta\theta} = (a_z^2 - 1)$. The eigenproblem (2.39) decouples, and the eigenvalues are given by

$$\mu_n = -n^2 + (1 - k^2 a_z^2), \quad (3.4)$$

with $H_n(\phi) = \cos n\phi$ or $\sin n\phi$ [c.f. Cahn (1979)]. For $a_z \gg 1$, there is a long-wavelength axisymmetric instability with $k_c = 1/a_z$. The unstable perturbations have wavelengths $\lambda > \pi(2a_z)$ that are longer than the length of the corresponding equilibrium shape, which is consistent with the underlying stability of the equilibrium shape. For $a_z \gg 1$, the surface energy for interface orientations with unit normal (n_x, n_y, n_z) is relatively low for small values of n_x and high near $n_z = 1$. This has the dual effect of producing equilibrium shapes that are highly elongated in the z -direction, and stabilizing the infinite cylinder to all but long-wavelength axial perturbations.

(c) Cubic Surface Energy

A simple model of the surface energy anisotropy for a cubic material is given by the dimensional expression (McFadden *et al.* 1988)

$$\gamma(n'_x, n'_y, n'_z) = \gamma_0 \{1 + 4\epsilon_4([n'_x]^4 + [n'_y]^4 + [n'_z]^4)\} \quad (3.5)$$

where we employ a primed coordinate system that is attached to the crystal axes. We will consider the high symmetry orientations [001], a four-fold axis; [011], a two-fold axis; and [111], a three-fold axis. We will use appropriate preliminary rotations of the crystal axes in each case to bring these axes into alignment with the z -axis of the rod, which will be fixed in the unprimed coordinate system.

In figure 3 we show examples of 3-D equilibrium shapes corresponding to the surface energy given in eq. (3.5). The shapes are smooth for $-1/18 < \epsilon_4 < 1/12$. For $\epsilon_4 < 0$ the shapes resemble rounded cubes, with [110] edges first forming at $\epsilon_4 = -1/18 \approx -0.0556$. As ϵ_4 decreases below $-1/18$, the edges extend toward the [111] directions, merging to form a corner for $\epsilon_4 = -5/68 \approx -0.07735$. For $\epsilon_4 > 0$ the shapes are octahedral, with [100] corners first forming at $\epsilon_4 = 1/12 \approx 0.0833$.

For numerical determination of the eigenvalues we used two different numerical methods. The first method used the Sturm-Liouville solver, SLEIGN2 (Bailey *et al.* 2001). The second method uses a pseudospectral discretization (Voigt *et al.* 1984) of the equations and then computes the eigenvalues of the resulting matrix by using the EISPACK solver RS (Smith *et al.* 1976) for real symmetric matrices. Both methods gave identical numerical results.

(i) [001] Orientation

If the axis of the rod is aligned with the [001] orientation of the crystal, then no preliminary rotation of the crystal is required, and the dimensionless surface energy resulting from eq. (3.5) is given by (Kessler & Levine 1987,1988; McFadden *et al.* 2000)

$$\gamma(\phi, \theta) = 1 + \epsilon_4 [4 \cos^4 \theta + \sin^4 \theta (3 + \cos 4\phi)]. \quad (3.6)$$

In the plane $\theta = \pi/2$, we then have $\gamma_{\theta\phi} = 0$, and

$$\gamma = (1 + 3\epsilon_4) + \epsilon_4 \cos 4\phi, \quad (3.7)$$

$$(\gamma + \gamma_{\phi\phi})(\gamma + \gamma_{\theta\theta}) = \left(1 - 6\epsilon_4 - \frac{9}{2}\epsilon_4^2\right) - (18\epsilon_4 - 126\epsilon_4^2) \cos 4\phi + \frac{45}{2}\epsilon_4^2 \cos 8\phi. \quad (3.8)$$

The rod is also smooth for $-1/18 \leq \epsilon_4 \leq 1/12$, and missing orientations occur for $\epsilon_4 < -1/18$ and $\epsilon_4 > 1/12$. Cross sections of the unperturbed rod over the range $-1/18 \leq \epsilon_4 \leq 1/12$ are shown in figure 4a.

Since the term $\gamma_{\theta\phi}$ vanishes, eq. (2.39) decouples and the eigenfunctions satisfy the equation

$$H_n''(\phi) + (1 - k^2 [1 + \epsilon_4 A_1(\phi) + \epsilon_4^2 A_2(\phi)]) H_n(\phi) = \mu_n H_n(\phi), \quad (3.9)$$

where

$$A_1(\phi) = -6[1 + 3 \cos 4\phi], \quad A_2(\phi) = -\frac{9}{2}[1 - 28 \cos 4\phi - 5 \cos 8\phi]. \quad (3.10)$$

Figure 4b shows the results of a numerical computation of the first three eigenvalues for $\epsilon_4 = 1/12$. There is a range $0 < k < k_c \approx 1.5$ where the first mode $H_0(\phi)$ is unstable with $\mu_0 > 0$; this mode corresponds to a continuation in ϵ_4 of the $n = 0$

axisymmetric mode for the isotropic case. All other modes are found to be stable for all wavenumbers.

A formal asymptotic expansion for $|\epsilon_4| \ll 1$ can be used to compute an approximation to the the eigenfunctions and eigenvalues. The solution is given by expanding $H_n(\phi)$ and μ_n in terms of ϵ_4 as

$$H_n(\phi) = H_n^{(0)}(\phi) + \epsilon_4 H_n^{(1)}(\phi) + \frac{\epsilon_4^2}{2} H_n^{(2)}(\phi) + \frac{\epsilon_4^3}{6} H_n^{(3)}(\phi) + O(\epsilon_4^4) \quad (3.11)$$

$$\mu_n = \mu_n^{(0)} + \epsilon_4 \mu_n^{(1)} + \frac{\epsilon_4^2}{2} \mu_n^{(2)} + \frac{\epsilon_4^3}{6} \mu_n^{(3)} + O(\epsilon_4^4), \quad (3.12)$$

where $H_n^{(0)}(\phi)$ and $\mu_n^{(0)}$ correspond to the isotropic case with $\epsilon_4 = 0$. We restrict attention to the most dangerous mode, corresponding to $n = 0$. The expansion gives

$$H_0(\phi) = 1 + \frac{9}{8} k^2 \epsilon_4 \cos 4\phi \left(1 + \frac{1}{32} \epsilon_4 \{ (9k^2 - 20) \cos 4\phi - 224 \} \right) + O(\epsilon_4^3), \quad (3.13)$$

$$\mu_0 = [1 - k^2] + 6k^2 \epsilon_4 + \frac{9}{8} k^2 (4 + 9k^2) \epsilon_4^2 - \frac{567}{4} k^4 \epsilon_4^3 + O(\epsilon_4^4). \quad (3.14)$$

As can be seen in figure 4a, the dimensionless area of the unperturbed rod's cross section varies with ϵ_4 ; it is given by

$$A(\epsilon_4) = \frac{1}{2} \int_0^{2\pi} \gamma(\gamma + \gamma_{\phi\phi}) d\phi = \pi \left(1 + 6\epsilon_4 + \frac{3}{2} \epsilon_4^2 \right) = \pi R_e^2, \quad (3.15)$$

where $R_e = \sqrt{1 + 6\epsilon_4 + 3\epsilon_4^2/2}$ is the effective radius of the cross section. To eliminate this change in length scale with ϵ_4 , we set $\kappa = kR_e$, which is the dimensionless axial wavenumber based on the effective radius of the cross section.

In figure 5a we show the most unstable mode over the range $-1/18 < \epsilon_4 < 1/12$ as a function of κ . The rod is stabilized for $\epsilon_4 < 0$ and destabilized for $\epsilon_4 > 0$. The square of the corresponding critical wavenumber κ_c as a function of ϵ_4 is shown as the solid curve in figure 5b; the wavenumber varies from $\kappa_c = 0.72639$ at $\epsilon_4 = -1/18$ to $\kappa_c = 1.8503$ at $\epsilon_4 = 1/12$. The dashed curve shows the corresponding result from the asymptotic expansion for small ϵ_4 , which takes the form

$$\kappa_c^2 = 1 + 12\epsilon_4 + \frac{705}{8} \epsilon_4^2 + \frac{2493}{4} \epsilon_4^3 + O(\epsilon_4^4). \quad (3.16)$$

(ii) [011] Orientation

If the axis of the rod is aligned with the [011] orientation of the crystal, then an appropriate rotation of the crystal axes relative to the rod axis is given by (McFadden *et al.* 1988)

$$\begin{pmatrix} n'_x \\ n'_y \\ n'_z \end{pmatrix} = \begin{pmatrix} 1 & 0 & 0 \\ 0 & 1/\sqrt{2} & 1/\sqrt{2} \\ 0 & -1/\sqrt{2} & 1/\sqrt{2} \end{pmatrix} \begin{pmatrix} n_x \\ n_y \\ n_z \end{pmatrix}, \quad (3.17)$$

as shown in figure 6.

This rotation gives

$$\gamma = 1 + 4\epsilon_4 \left(n_x^4 + \frac{n_y^4}{2} + \frac{n_z^4}{2} + 3n_y^2 n_z^2 \right), \quad (3.18)$$

which reduces to

$$\gamma = 1 + 2\epsilon_4 (\cos^4 \theta + 6 \cos^2 \theta \sin^2 \theta \sin^2 \phi + 2 \sin^4 \theta \cos^4 \phi + \sin^4 \theta \sin^4 \phi). \quad (3.19)$$

In the plane $\theta = \pi/2$, we then have $\gamma_{\theta\phi} = 0$, and

$$\gamma = \left(1 + \frac{9}{4}\epsilon_4 \right) + \epsilon_4 \cos 2\phi + \frac{3}{4}\epsilon_4 \cos 4\phi, \quad (3.20)$$

$$\begin{aligned} (\gamma + \gamma_{\phi\phi})(\gamma + \gamma_{\theta\theta}) &= \left(1 + \frac{3}{2}\epsilon_4 [5 - 12 \cos 2\phi - 9 \cos 4\phi] + \right. \\ &\left. \frac{9}{32}\epsilon_4^2 [167 + 136 \cos 2\phi - 148 \cos 4\phi + 312 \cos 6\phi + 45 \cos 8\phi] \right). \end{aligned} \quad (3.21)$$

The rod is smooth for $-5/68 \leq \epsilon_4 \leq 1/12$, which is a larger range than the [001] case. Cross sections of the unperturbed rod are shown in figure 7a. Missing orientations on the rod occur for $\epsilon_4 < -5/68$ and $\epsilon_4 > 1/12$.

Over the range $\epsilon_4 = -5/68 \approx -0.0735$ to $\epsilon_4 = -1/18 \approx -0.0556$ the rod is smooth ($\gamma + \gamma_{\phi\phi} > 0$), but edges have formed on the 3-D equilibrium shape. In the variables of eq. (3.19), this edge is a discontinuity in slope in the θ -direction in the plane $\theta = \pi/2$, with $\gamma + \gamma_{\theta\theta} < 0$ near $\phi = \pm\pi/2$. The edges are smooth in ϕ , however, until they merge to form the corner seen in the innermost curve in figure 7a for $\epsilon_4 = -5/68$.

Since the term $\gamma_{\theta\phi}$ vanishes, eq. (2.39) decouples and the eigenfunctions satisfy the analogous version of eq. (3.9), with the corresponding coefficients $A_1(\phi)$ and $A_2(\phi)$ given by eq. (3.21). We first note that over the range $-5/68 < \epsilon_4 < -1/18$, there is a large-wavenumber instability associated with $\gamma + \gamma_{\theta\theta} < 0$. Dispersion curves for $\epsilon_4 = -0.060$ are shown in figure 7. The $n = 0$ mode has two values of k_c with $\mu = 0$, and is increasingly unstable for large wavenumbers with $\mu \approx 0.11k^2$. For $k \gg 1$ these modes are concentrated near the minima in $\gamma + \gamma_{\theta\theta}$ near $\phi = \pi/2$ and $\phi = 3\pi/2$ as shown in figure 8. A WKB analysis suggests a large-wavenumber dependence of the form $\mu = k^2[\mu_0 + O(1/k)]$, where $\mu_0 = -\min(\gamma + \gamma_{\phi\phi})(\gamma + \gamma_{\theta\theta})$. For $\epsilon_4 = -0.06$, this gives $\mu_0 = 0.1088$, in good agreement with the numerical calculations.

For $-1/18 < \epsilon_4 < 1/12$ the results are qualitatively similar to the [001] case; there is again a single unstable mode with $n = 0$ corresponding to the continuation in ϵ_4 of the $n = 0$ axisymmetric mode for the isotropic case. All other modes are found to be stable for all wavenumbers.

For $|\epsilon_4| \ll 1$ the $n = 0$ mode is given by

$$\begin{aligned} H_0(\phi) &= 1 + \frac{9}{2}\epsilon_4 k^2 (\cos 2\phi + \frac{3}{16} \cos 4\phi) + \frac{9}{128} k^2 \epsilon_4^2 \left((135k^2 - 136) \cos 2\phi + \right. \\ &\quad \left. (36k^2 + 37) \cos 4\phi + \frac{1}{3}(45k^2 - 104) \cos 6\phi + \right. \\ &\quad \left. \frac{9}{64}(9k^2 - 20) \cos 8\phi \right) + O(\epsilon_4^3), \end{aligned} \quad (3.22)$$

$$\begin{aligned} \mu_0 = & [1 - k^2] - \frac{15}{2}k^2\epsilon_4 + \frac{9}{128}k^2(657k^2 - 668)\epsilon_4^2 + \\ & \frac{81}{256}k^4(324k^2 - 433)\epsilon_4^3 + O(\epsilon_4^4). \end{aligned} \quad (3.23)$$

As can be seen in figure 7a the dimensionless area of the unperturbed rod's cross section varies with ϵ_4 ; it is given by

$$A(\epsilon_4) = \frac{1}{2} \int_0^{2\pi} \gamma(\gamma + \gamma_{\phi\phi}) d\phi = \pi \left(1 + \frac{9}{2}\epsilon_4 - \frac{21}{32}\epsilon_4^2 \right) = \pi R_e^2; \quad (3.24)$$

we again rescale by setting $\kappa = kR_e$. In figure 9a we show the most unstable mode over the range $-1/18 < \epsilon_4 < 1/12$ as a function of κ . In contrast to the [001] case, for the [011] case the rod is destabilized for $\epsilon_4 < 0$ and stabilized for $\epsilon_4 > 0$. The square of the corresponding critical wavenumber κ_c as a function of ϵ_4 is shown as the solid curve in figure 9b. The curve is double-valued for $\epsilon_4 < -1/18$ (c.f. figure 7b) with a limit point at $\epsilon_4 \approx -0.0638$ and $\kappa_c \approx 2$; only the lower branch is shown. The dashed curve shows the corresponding result from the asymptotic expansion for small ϵ_4 , which takes the form

$$\kappa_c^2 = 1 - 3\epsilon_4 + \frac{2697}{128}\epsilon_4^2 - \frac{137385}{256}\epsilon_4^3 + O(\epsilon_4^4). \quad (3.25)$$

(iii) [111] Orientation

If the axis of the rod is aligned with the [111] orientation of the crystal, then an appropriate rotation of the crystal axes relative to the rod axis is given by (McFadden *et al.* 1988)

$$\begin{pmatrix} n'_x \\ n'_y \\ n'_z \end{pmatrix} = \begin{pmatrix} \sqrt{2}/\sqrt{3} & 0 & 1/\sqrt{3} \\ -1/\sqrt{6} & 1/\sqrt{2} & 1/\sqrt{3} \\ -1/\sqrt{6} & -1/\sqrt{2} & 1/\sqrt{3} \end{pmatrix} \begin{pmatrix} n_x \\ n_y \\ n_z \end{pmatrix}, \quad (3.26)$$

as shown in figure 3.

This leads to the form

$$\begin{aligned} \gamma = & 1 + 4\epsilon_4 \left(\frac{n_x^4}{2} + \frac{n_y^4}{2} + \frac{n_z^4}{3} + n_x^2 n_y^2 + 2n_x^2 n_z^2 + 2n_y^2 n_z^2 \right. \\ & \left. + \frac{2\sqrt{2}}{3} n_x^3 n_z - 2\sqrt{2} n_x n_y^2 n_z \right), \end{aligned} \quad (3.27)$$

which reduces to

$$\gamma = 1 + 4\epsilon_4 \left(\frac{1}{3} \cos^4 \theta + 2 \cos^2 \theta \sin^2 \theta + \frac{1}{2} \sin^4 \theta + \frac{2\sqrt{2}}{3} \cos \theta \sin^3 \theta \cos 3\phi \right). \quad (3.28)$$

In the plane $\theta = \pi/2$, we then have

$$\gamma = 1 + 2\epsilon_4, \quad (3.29)$$

so that the surface energy is isotropic in this plane, leading to a circular cross section of radius $R_e = 1 + 2\epsilon_4$. (We must have $\epsilon_4 > -1/2$ to maintain a positive surface energy.) In this plane we also have

$$\gamma_{\theta\phi} = 8\sqrt{2}\epsilon_4 \sin 3\phi, \quad (3.30)$$

so that eq. (2.39) does not decouple. We also have

$$\gamma + \gamma_{\theta\theta} = 1 + 10\epsilon_4, \quad (3.31)$$

so that $(\gamma + \gamma_{\phi\phi})(\gamma + \gamma_{\theta\theta}) = (1 + 2\epsilon_4)(1 + 10\epsilon_4)$ is negative for $-1/2 < \epsilon_4 < -1/10$.

We have the following system of equations:

$$\begin{aligned} \frac{d^2 H_n}{d\phi^2} + [1 - k^2 (1 + 12\epsilon_4 + 20\epsilon_4^2)] H_n + 16\sqrt{2}k\epsilon_4 \sin(3\phi) \frac{dG_n}{d\phi} + \\ 24\sqrt{2}k\epsilon_4 \cos(3\phi) G_n = \mu_n H_n, \end{aligned} \quad (33)$$

$$\begin{aligned} \frac{d^2 G_n}{d\phi^2} + [1 - k^2 (1 + 12\epsilon_4 + 20\epsilon_4^2)] G_n - 16\sqrt{2}k\epsilon_4 \sin(3\phi) \frac{dH_n}{d\phi} - \\ 24\sqrt{2}k\epsilon_4 \cos(3\phi) H_n = \mu_n G_n. \end{aligned} \quad (34)$$

For $|\epsilon_4| \ll 1$ we find an approximate solution for $n = 0$ of the form

$$\begin{aligned} h(\phi, z) = \sin kz \left[1 - \frac{16}{3} k^2 \epsilon_4^3 \cos(6\phi) + O(\epsilon_4^4) \right] \\ - \cos kz \left[\frac{8\sqrt{2}}{3} k\epsilon_4 \cos(3\phi) + O(\epsilon_4^4) \right], \end{aligned} \quad (3.35)$$

$$\mu_0 = (1 - k^2) - 12k^2\epsilon_4 + 44k^2\epsilon_4^2 + O(\epsilon_4^3). \quad (3.36)$$

Another equivalent solution is given by a translation in z by π/k . A schematic plot of the perturbed cylinder corresponding to eq. (3.35) is shown in figure 11a. The perturbed shape lacks any planes of symmetry normal to the z -axis, and exhibits the three-fold symmetry in ϕ expected for a cylinder in the [111] direction.

A numerical calculation of the square of the critical wavenumber for the $n = 0$ mode over the range $-1/18 < \epsilon_4 < 1/12$ is shown in figure 11b. The rod is destabilized for $\epsilon_4 < 0$ and stabilized for $\epsilon_4 > 0$. The rational approximation

$$\kappa_c^2 = \frac{(1 + 2\epsilon_4)^2}{(1 + 12\epsilon_4 - 44\epsilon_4^2)} \quad (3.37)$$

obtained from eq. (3.36) is also shown as a dashed curve in this figure, but the results are indistinguishable from the numerical results to graphical accuracy. For anisotropies $\epsilon_4 < -1/18$ for which the 3-D equilibrium shape has developed edges, we find more complicated dispersion relations indicating multiple bifurcations of several of the eigenmodes.

4. Discussion

The second variation of the energy of the perturbed rod involves the terms $\gamma_{\theta\phi}$ and $(\gamma + \gamma_{\phi\phi})(\gamma + \gamma_{\theta\theta})$. The latter product is evocative of a weighted Gauss curvature, in the following sense. The first variation of a general anisotropic surface energy leads to the weighted mean curvature, which can be expressed via the Herring formula (1951)

$$\frac{(\gamma + \gamma_{\theta_1\theta_1})}{R_1} + \frac{(\gamma + \gamma_{\theta_2\theta_2})}{R_2} = \nabla_S \cdot \vec{\xi}. \quad (4.1)$$

Here $1/R_j = \kappa_j$ are the principal curvatures of a general surface, $\vec{X}(u_1, u_2)$, expressed in terms of principal coordinates u_j (O'Neill 1966). The angles θ_j measure the local orientation of the surface, and their variation with arclength along u_j satisfy $d\theta_j = \kappa_j ds$. The unit normal vector $\hat{N}(u_1, u_2)$ satisfies Rodrigue's formula (Abram 1965), $\partial \hat{N} / \partial u_j = \kappa_j \partial \vec{X} / \partial u_j$, for $j = 1, 2$.

For the case of isotropic surface energy, the first and second variations of the energy involve the usual mean curvature $\mathcal{K} = (\kappa_1 + \kappa_2)$ and Gauss curvature $\mathcal{G} = \kappa_1 \kappa_2$. This is illustrated by considering a normal variation $\vec{x}(u_1, u_2) = \vec{X}(u_1, u_2) + \epsilon \hat{N}(u_1, u_2)$, which has a vector area element given by (O'Neill 1966)

$$\left(\frac{\partial \vec{x}}{\partial u_1} \times \frac{\partial \vec{x}}{\partial u_2} \right) du_1 du_2 = \left(\frac{\partial \vec{X}}{\partial u_1} \times \frac{\partial \vec{X}}{\partial u_2} \right) [1 + \epsilon \mathcal{K} + \epsilon^2 \mathcal{G}] du_1 du_2, \quad (4.2)$$

which follows from Rodrigue's formula. Our stability equation, derived by taking the second variation of the energy for the perturbed rod, involves the product of the same terms, $(\gamma + \gamma_{\phi\phi})$ and $(\gamma + \gamma_{\theta\theta})$, that appear in Herring's formula for the first variation of the energy, which is suggestive of the appearance of a weighted Gauss curvature.

We have considered an energy argument to determine the critical wavenumbers of perturbations that lower the total energy of the rod. This analysis takes into account only the surface energy of the interface and is not tied to a specific time-dependent process that would describe the subsequent temporal evolution of the interface. A time-dependent analysis would require consideration of a specific model for the dynamics of the process, which we have avoided in our treatment. On the other hand, such considerations are necessary to determine realistic time-scales for the evolution that are related to the maximum growth rates predicted by a linear theory (see, e.g., McFadden *et al.* 1993; Nichols & Mullins 1965); our treatment does not provide estimates for growth rates.

The cubic surface energy example leads to a situation in which the surface energy anisotropy may be high enough that the 3-D equilibrium is missing orientations, while the 2-D cross section of the rod remains smooth, with $(\gamma + \gamma_{\phi\phi}) > 0$. For example, if the rod is aligned in the [111] direction, a circular cross section is the 2-D equilibrium shape for all levels of anisotropy; the corresponding 2-D surface energy $\gamma(\phi, \pi/2)$ is isotropic. This is a result of the special fourth-order form that we have assumed for the surface energy in eq. (3.5); a more general expression that includes sixth-order terms (McFadden *et al.* 1988),

$$\gamma(n'_x, n'_y, n'_z) = 1 + 4\epsilon_4 ([n'_x]^4 + [n'_y]^4 + [n'_z]^4) + 6\epsilon_6 ([n'_x]^6 + [n'_y]^6 + [n'_z]^6) \quad (4.3)$$

leads to an anisotropic 2-D surface energy $\gamma(\phi, \pi/2) = (1 + \epsilon_6 \cos 6\phi)$ for a rod aligned in the [111] direction, and the corresponding 2-D cross section has six-fold symmetry.

We have considered a single model of a cubic surface energy anisotropy characterized by the parameter ϵ_4 in eq. (3.5). We have obtained results for the critical wavenumber for high-symmetry orientations of the rod over the range $-1/18 \leq \epsilon_4 \leq 1/12$ for which the 3-D equilibrium shape remains smooth in this model. This is a reasonable range of values for many metallic systems and for several transparent organics that are often used as non-faceting model systems to study solidification. Typical values of surface energy anisotropy in such systems are on the order of a few percent (see the tabulated values for cubic materials in Napolitano *et al.* in press). Both experimental measurements (e.g., Glicksman & Singh 1989) and computational techniques (e.g., Hoyt *et al.* 2001) have been used to obtain estimates for surface energy anisotropy.

We have restricted our attention to anisotropies that are mild enough that no orientations are missing on the unperturbed rod. It would be valuable to extend the analysis to stronger anisotropies for which missing orientations do occur. This would require explicit consideration of the Weierstrass-Erdmann corner conditions (Bolza 1961) that characterize a change in slope on the equilibrium solution. Another approach would be to introduce regularizing terms (Gurtin 1993; Golovin *et al.* 1998) associated with edge energies to smooth out the corners.

We have found that surface energy anisotropy can play a significant role in determining the stability of a rod or wire which is assumed to be isolated from surrounding solid surfaces. It would be valuable to extend the analysis to take into account effects of a substrate in contact with the rod. An analysis of capillary instabilities of a thin solid film on a substrate that takes into account the effect of isotropic surface energies on the contact line of the film has been performed by McCallum *et al.* (McCallum *et al.* 1996). We are currently extending this work to include the effects of surface energy anisotropy.

5. Conclusion

We have examined the linear stability of a rod or wire with a uniform cross section given by a 2-D equilibrium shape. The analysis is based on computing the sign of the second variation of the energy, which is examined by solving an associated eigenvalue problem. The eigenvalues may be determined numerically or, in the limit of small anisotropy, by an asymptotic expansion. The eigenproblem is a coupled pair of second-order ordinary differential equations with periodic coefficients that depend on the second derivatives of the surface energy with respect to orientation variables. In this study the surface energy anisotropy is assumed to be sufficiently weak that no missing orientations are present on the rod. We have included discussion of examples with uniaxial or cubic anisotropy, which illustrate that anisotropic surface energy plays a significant role in the stability of a rod. Both the magnitude and sign of the anisotropy determine whether the contribution stabilizes or destabilizes the system relative to the case of isotropic surface energy, which reproduces the classical Rayleigh instability.

Appendix I

Here we derive the expressions in eq. (2.23). To simplify the notation we denote the cartesian components of the normal vector by $\vec{P} = (u, v, w)$, and write

$$\Gamma(u, v, w) = \sqrt{u^2 + v^2 + w^2} \gamma(\Phi, \Theta), \quad (5.1)$$

where

$$\tan \Phi = \frac{v}{u}, \quad \tan \Theta = \frac{\sqrt{u^2 + v^2}}{w}. \quad (5.2)$$

The first derivatives of $\Gamma(u, v, w)$, evaluated in the plane $w = 0$, are given by

$$\Gamma_u(u, v, 0) = \frac{u}{A} \gamma - \frac{v}{A} \gamma_\Phi, \quad (5.3)$$

$$\Gamma_v(u, v, 0) = \frac{v}{A} \gamma + \frac{u}{A} \gamma_\Phi, \quad (5.4)$$

$$\Gamma_w(u, v, 0) = -\gamma_\Theta, \quad (5.5)$$

where $A^2 = u^2 + v^2$.

The second derivatives of $\Gamma(u, v, w)$ in the plane $w = 0$ reduce to

$$\Gamma_{uu}(u, v, 0) = \frac{v^2}{A^3} [\gamma + \gamma_{\phi\phi}], \quad (5.6)$$

$$\Gamma_{uv}(u, v, 0) = \frac{-uv}{A^3} [\gamma + \gamma_{\phi\phi}], \quad (5.7)$$

$$\Gamma_{vv}(u, v, 0) = \frac{u^2}{A^3} [\gamma + \gamma_{\phi\phi}], \quad (5.8)$$

$$\Gamma_{uw}(u, v, 0) = \frac{v}{A^2} \gamma_{\theta\phi}, \quad (5.9)$$

$$\Gamma_{vw}(u, v, 0) = \frac{-u}{A^2} \gamma_{\theta\phi}, \quad (5.10)$$

$$\Gamma_{ww}(u, v, 0) = \frac{1}{A} [\gamma + \gamma_{\theta\theta}]. \quad (5.11)$$

For the expansion in eq. (2.23), the arguments are evaluated at $\theta = \pi/2$, and the appropriate values for u and v correspond to $\vec{P}^{(0)}$, with $u = (\gamma + \gamma_{\phi\phi}) \cos \phi$, $v = (\gamma + \gamma_{\phi\phi}) \sin \phi$, and $w = 0$. We therefore find that

$$\Gamma(\vec{P}^{(0)}) = \gamma(\gamma + \gamma_{\phi\phi}), \quad (5.12)$$

and

$$\vec{\xi}^{(0)}(\phi) = \Gamma_u \hat{x} + \Gamma_v \hat{y} + \Gamma_w \hat{z} = \gamma \hat{r} + \gamma_\phi \hat{\phi} - \gamma_\theta \hat{z}. \quad (5.13)$$

The cartesian components of $\vec{\xi}^{(1)}$ are given by

$$\xi_j^{(1)} = \sum_{k=1}^3 \Gamma_{u_j u_k} P_k^{(1)} \quad (5.14)$$

where the second derivatives of Γ are given above, and P_k are the cartesian components of the perturbed normal vector $\vec{P}^{(1)}$ given in eq. (2.5). Evaluating the sums gives

$$\vec{\xi}^{(1)}(\phi) = [\gamma_{\theta\phi}h_z - h_\phi] \hat{\phi} + \left[\frac{\gamma_{\theta\phi}h_\phi}{(\gamma + \gamma_{\phi\phi})} - (\gamma + \gamma_{\theta\theta})h_z \right] \hat{z}. \quad (5.15)$$

Appendix II

The linear operator in eq. (2.34),

$$Lh = h_{\phi\phi} + h + (\gamma + \gamma_{\phi\phi})(\gamma + \gamma_{\theta\theta})h_{zz} - \gamma_{\theta\phi}h_{z\phi} - [\gamma_{\theta\phi}h_z]_\phi \quad (5.1)$$

in the eigenproblem can be interpreted as the linearized form of the weighted mean curvature $\nabla_S \cdot \vec{\xi}$. To see this, note that for a shape of the form

$$\vec{X}(\phi, z) = \gamma\hat{r} + \gamma_\phi\hat{\phi} + z\hat{z} + \epsilon h(\phi, z)\hat{r} + O(\epsilon^2), \quad (5.2)$$

we can write (Weatherburn 1927)

$$\nabla_S \cdot \vec{\xi} = \vec{T}_\phi \cdot \frac{\partial \vec{\xi}}{\partial \phi} + \vec{T}_z \cdot \frac{\partial \vec{\xi}}{\partial z}, \quad (5.3)$$

where \vec{T}_ϕ and \vec{T}_z are tangent vectors that are bi-orthogonal to the tangent vectors $\partial \vec{X}/\partial \phi$ and $\partial \vec{X}/\partial z$,

$$\vec{T}_\phi \cdot \frac{\partial \vec{X}}{\partial \phi} = 1, \quad \vec{T}_\phi \cdot \frac{\partial \vec{X}}{\partial z} = 0. \quad (5.4)$$

$$\vec{T}_z \cdot \frac{\partial \vec{X}}{\partial \phi} = 0, \quad \vec{T}_z \cdot \frac{\partial \vec{X}}{\partial z} = 1. \quad (5.5)$$

Expanding through first order in ϵ gives

$$\begin{aligned} \nabla_S \cdot \vec{\xi} &= \left\{ \vec{T}_\phi^{(0)} \cdot \frac{\partial \vec{\xi}^{(0)}}{\partial \phi} + \vec{T}_z^{(0)} \cdot \frac{\partial \vec{\xi}^{(0)}}{\partial z} \right\} \\ &+ \epsilon \left\{ \vec{T}_\phi^{(0)} \cdot \frac{\partial \vec{\xi}^{(1)}}{\partial \phi} + \vec{T}_z^{(0)} \cdot \frac{\partial \vec{\xi}^{(1)}}{\partial z} + \vec{T}_\phi^{(1)} \cdot \frac{\partial \vec{\xi}^{(0)}}{\partial \phi} + \vec{T}_z^{(1)} \cdot \frac{\partial \vec{\xi}^{(0)}}{\partial z} \right\} + O(\epsilon^2). \end{aligned} \quad (5.6)$$

We have

$$\frac{\partial \vec{X}}{\partial \phi} = (\gamma + \gamma_{\phi\phi})\hat{\phi} + \epsilon \{ h_\phi \hat{r} + h\hat{\phi} \} + O(\epsilon^2), \quad (5.7)$$

$$\frac{\partial \vec{X}}{\partial z} = \hat{z} + \epsilon h_z \hat{r} + O(\epsilon^2), \quad (5.8)$$

$$\vec{T}_\phi = \frac{1}{(\gamma + \gamma_{\phi\phi})} \hat{\phi} - \frac{\epsilon}{(\gamma + \gamma_{\phi\phi})^2} \{h\hat{\phi} + h_\phi \hat{r}\} + O(\epsilon^2), \quad (5.9)$$

$$\vec{T}_z = \hat{z} + O(\epsilon), \quad (5.10)$$

$$\vec{\xi} = \gamma \hat{r} + \gamma_\phi \hat{\phi} - \gamma_\theta \hat{z} + \epsilon \left\{ [\gamma_\theta h_z - h_\phi] \hat{\phi} + \left[\frac{\gamma_\theta h_\phi}{(\gamma + \gamma_{\phi\phi})} - (\gamma + \gamma_\theta) h_z \right] \hat{z} \right\} + O(\epsilon^2) \quad (5.11)$$

We then find

$$\vec{T}_\phi^{(1)} \cdot \frac{\partial \vec{\xi}^{(0)}}{\partial \phi} + \vec{T}_z^{(1)} \cdot \frac{\partial \vec{\xi}^{(0)}}{\partial z} = \frac{-h}{(\gamma + \gamma_{\phi\phi})}, \quad (5.12)$$

and

$$\vec{T}_\phi^{(0)} \cdot \frac{\partial \vec{\xi}^{(1)}}{\partial \phi} + \vec{T}_z^{(0)} \cdot \frac{\partial \vec{\xi}^{(1)}}{\partial z} = \frac{[\gamma_\theta h_z]_\phi - h_{\phi\phi}}{(\gamma + \gamma_{\phi\phi})} + \frac{\gamma_\theta h_\phi h_{\phi z}}{(\gamma + \gamma_{\phi\phi})} - (\gamma + \gamma_\theta) h_{zz}. \quad (5.13)$$

Combining these results gives

$$\begin{aligned} \nabla_S \cdot \vec{\xi} &= 1 - \frac{\epsilon \left\{ h - [\gamma_\theta h_z]_\phi + h_{\phi\phi} - \gamma_\theta h_\phi h_{\phi z} + (\gamma + \gamma_{\phi\phi})(\gamma + \gamma_\theta) h_{zz} \right\}}{(\gamma + \gamma_{\phi\phi})} + O(\epsilon^2), \\ &= 1 - \frac{\epsilon}{(\gamma + \gamma_{\phi\phi})} Lh + O(\epsilon^2). \end{aligned} \quad (5.14)$$

The authors are grateful for helpful discussions with S.H. Davis, who suggested the work, J.W. Cahn, S.R. Coriell, A. Dienstfrey, A. Golovin, M.J. Miksis, and P.W. Voorhees. The first author was supported by a National Research Council Postdoctoral Fellowship, and the second author was supported by the Microgravity Research Division of NASA. Part of this research was performed at Northwestern University with the support of the NSF Nanoscale Interdisciplinary Research Teams Program under grant number DMR-0102794.

References

- Abram, J. 1965 *Tensor Calculus through Differential Geometry*. London: Butterworths.
- Bailey, P. B., Everitt, W. N., & Zettl, A. 2001 Algorithm 810: The SLEIGN2 Sturm-Liouville code, *ACM T Math Software* **27** (2), 143-192.
- Bolza, O. 1961 *Lectures on the Calculus of Variations*. New York: Dover.
- Brattkus, K. 1989 Capillary instabilities in deep cells during directional solidification. *J. Phys.-Paris* **50** (19), 2999-3006.
- Cahn, J. W. 1979 Stability of Rods with Anisotropic Surface Free Energy. *Scripta Metall.* **13**, 1069-1071.
- Cahn, J. W. & Hoffmann, D. W. 1974 A vector thermodynamics for anisotropic interfaces. II. Curved and faceted surfaces. *Acta Metall.* **22**, 1205-1214.
- Chen, Y., Ohlberg, D. A. A., Medeiros-Ribeiro, G., Chang, Y.A. & Williams, R. S. 2000. Self-assembled growth of epitaxial erbium disilicide nanowires on silicon(001). *App. Phys. Lett.* **76**, 4004-4006.

- Chandrasekhar, S. 1961. *Hydromagnetic and Hydrodynamic Stability*, Ch. 12. Dover: New York.
- Chen, Y., Ohlberg, D. A. A. & Williams, R. S. 2001 Epitaxial growth of erbium silicide nanowires on silicon(001). *Mat. Sci. Eng.* B87 222-226.
- Coriell, S. R., Hardy, S. C. & Cordes, M. R. 1977 Stability of liquid zones. *J. Coll. Int. Sci.* 60, 126-136.
- Forest, M. G. & Wang, Q. 1998 Anisotropic microstructure-induced reduction of the Rayleigh instability for liquid crystalline polymers. *Phys. Lett. A* 245, 518-526.
- Fukunaga, A., Chu, S. & McHenry, M. E. 1998 Synthesis, structure, and superconducting properties of tantalum carbide nanorods and nanoparticles. *J. Mater. Res.* 13, 2465-2471.
- Glicksman, M. E. & Singh, N.B. 1989 Effects of crystal-melt energy anisotropy on dendritic morphology and growth kinetics. *J. Crystal Growth* 98, 277-284.
- Golovin, A. A., Davis, S. H. & Nepomnyashchy, A. A. 1998 A convective Cahn-Hilliard Model for the formation of facets and corners in crystal growth. *Physica D* 122, 202-230.
- Gurtin, M. E. 1993 *Thermomechanics of Evolving Phase Boundaries in the Plane*. Oxford: Clarendon Press.
- Herring, C. 1951 Surface tension as a motivation for sintering. In *The Physics of Powder Metallurgy*, (ed. W. E. Kingston), pp.143-179. New York: McGraw-Hill, New York.
- Herring, C. 1953 The use of classical macroscopic concepts in surface-energy problems. In *Structure and Properties of Solid Surfaces*, (eds R. Gomer and C. S. Smith), pp. 5-72. Chicago: University of Chicago Press.
- Hoffmann, D. W. & Cahn, J. W. 1972 A vector thermodynamics for anisotropic interfaces. I. Fundamentals and applications to plane surface junctions. *Surf. Sci.* 31 368-388.
- Hohman, M. M., Shin, M., Rutledge, G. & Brenner, M.P. 2001 Electrospinning and electrically forced jets. I. Stability theory. *Phys. Fluids* 13, 2201-2220.
- Hoyt, J. J., Asta, M. & Karma, A. 2001 Method for computing the anisotropy of the solid-liquid interfacial free energy. *Phys. Rev. Lett.* 86, 5530-5533.
- Johnson, C. A. & Chakerian, G. D. 1965 On the proof and uniqueness of Wulff's construction of the shape of minimum surface energy. *J. Math. Phys.* 6, 1403-1404.
- Kassubek, F., Stafford, C. A., Grabert, H. & Goldstein, R. E. 2001 Quantum suppression of the Rayleigh instability in nanowires. *Nonlinearity* 14, 167-177.
- Kessler, D. A. & Levine H. 1987 Growth velocity of three-dimensional dendritic crystals. *Phys. Rev. A* 36, 4123-4126.
- Kessler, D. A. & Levine, H. 1988 Pattern selection in three dimensional dendritic growth. *Acta Metall.* 36, 2693-2706.
- Kondo Y. & Takayanagi, K. 1997 Gold nanobridge stabilized by surface structure. *Phys. Rev. Lett.* 79, 3455-3458.
- Loretto, D., Ross, F. M. & Lucas, C. A. 1996 Quasi-one-dimensional CaF₂ islands formed on Si(001) by molecular beam epitaxy. *Appl. Phys. Lett.* 68, 2363-2365.
- Lowry, B. J. & Steen, P. H. 1997 Stability of slender liquid bridges subjected to axial flows. *J. Fluid Mech.* 330, 189-213.
- Majumdar, B. & Chattopadhyay, K. 1996 The Rayleigh instability and the origin of rows of droplets in the monotectic microstructure of zinc-bismuth alloys. *Met. Mat. Trans. A* 27, 2053-2057.
- Marinis, R. F. & Sekerka, R. F. 1979 A model for capillary-induced instabilities in directionally solidified eutectic alloys. In *Proceedings of the Conference on In Situ Composites - III, Materials Research Society Annual Meeting, Boston, MA, November 1978*, (eds J. L. Walter, M. F. Gigliotti, B. F. Oliver, & H. Bibring), pp. 86-94.
- McCallum, M. S., Voorhees, P. W., Miksis, M. J., Davis, S. H. & Wong, H. 1996 Capillary instabilities in solid thin films: Lines. *J. Appl. Phys.* 79, 7604-7611.

- McFadden, G. B., Coriell, S. R. & Murray, B. T. 1993 The Rayleigh instability for a cylindrical crystal-melt interface. In *Variational and Free Boundary Problems*, (eds A. Friedman & J. Spruck). The IMA Series in Mathematics and Its Applications, Volume 53, pp. 159-169. New York: Springer-Verlag.
- McFadden, G. B., Coriell, S. R., & Sekerka, R. F. 1988 Effect of surface tension anisotropy on cellular morphologies. *J. Crystal Growth* **91**, 180-198.
- McFadden, G. B., Coriell, S. R. & Sekerka, R. F. 2000 Effect of surface free energy anisotropy on dendrite tip shape. *Acta Mater.* **48**, 3177-3181.
- Migler, K. B. 2001 String Formation in sheared polymer blends: coalescence, breakup, and finite size effects. *Phys. Rev. Lett.* **86**, 1023-1026.
- Mullins, W. W. 1963 Solid surface morphologies governed by capillarity. In *Metal Surfaces: Structure, Energetics, and Kinetics*, pp. 17-66. Metals Park, OH: ASM.
- Napolitano, R.E., Liu, S. & Trivedi, R. 2002 Experimental measurement of anisotropy in crystal-melt interfacial energy. In press, *Interface Science*.
- Nichols F. A. & Mullins, W. W. 1965 Morphological changes of a surface of revolution due to capillary-induced surface diffusion. *J. Appl. Phys.* **36**, 1826-1835.
- O'Neill, B. 1966 *Elementary Differential Geometry*. New York: Academic Press.
- Pimbley, W. T. & Lee, H. C. 1977 Satellite droplet formation in a liquid jet. *IBM J. Res. Develop.* **21**, 21-30.
- Plateau, J. 1873 Experimental and theoretical researches on the figures of equilibrium of a liquid mass. . . (Transl. in *Annual Reports of the Smithsonian Institution*, 1863-1866.)
- Lord Rayleigh, 1878 On the instabilities of jets. *P. Lond. Math. Soc.* **10**, 4-13.
- Rottman C. & Wortis, M. 1984 Statistical mechanics of equilibrium crystal shapes: interfacial phase diagrams and phase transitions. *Phys. Rep.* **103**, 59-79.
- Slobozhanin, L. A., Alexander, J. I. D. & Resnick, A. H. 1997 Bifurcation of the equilibrium states of a weightless liquid bridge. *Phys. Fluids* **9**, 1893-1905.
- Smith, B. T., Boyle, J. M., Dongarra, J. J., Garbow, B. S., Ikebe, Y. Klema, V. C., Moler, C. B. 1976 *Matrix Eigensystem Routines - EISPACK Guide*, 2nd ed. New York: Springer-Verlag.
- Sundaram, M., Chalmers, S. A., Hopkins, P.F. & Gossard, A.C. 1991 New Quantum Structures. *Science* **254**, 1326-1335.
- Sutton A. P. & Balluffi, R. W. 1995 *Interfaces in Crystalline Materials*, Ch. 1. Oxford: Oxford University Press.
- Taylor, G. I. 1934 The formation of emulsions in definable fields of flow. *Proc. Roy. Soc. London*, A **146**, 501-533.
- Taylor, J. E. 1992 Mean curvature and weighted mean curvature. *Acta Metall. Mater.* **40**, 1475-1485.
- Tomotika, S. 1936 Breaking up of a drop of viscous liquid immersed in another viscous fluid which is extending at a uniform rate. *Proc. Roy. Soc. London* A **153**, 322-318.
- Voigt, R. G., Gottlieb, D. & Hussaini, M.Y. 1984 *Spectral Methods for Partial Differential Equations*, Philadelphia:SIAM.
- Voorhees, P. W., Coriell, S. R., McFadden, G. B. & Sekerka, R. F. 1984 The effect of anisotropic crystal-melt surface tension on grain boundary groove morphology. *J. Cryst. Growth* **67**, 425-440.
- Weatherburn, C. E. 1927 *Differential geometry of three dimensions*. Cambridge: Cambridge University Press.
- Zhang, Y. Q. & Alexander, J. I. D. 1990 Sensitivity of liquid bridges subject to axial residual acceleration. *Phys. Fluids* A **11** 1966-1974.

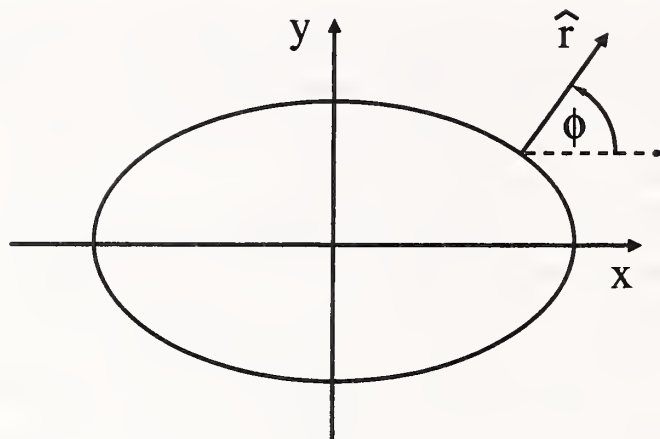


Figure 1. Schematic diagram of the 2-D equilibrium shape $x = X(\phi)$, $y = Y(\phi)$, with unit normal vector $\hat{r}(\phi)$.

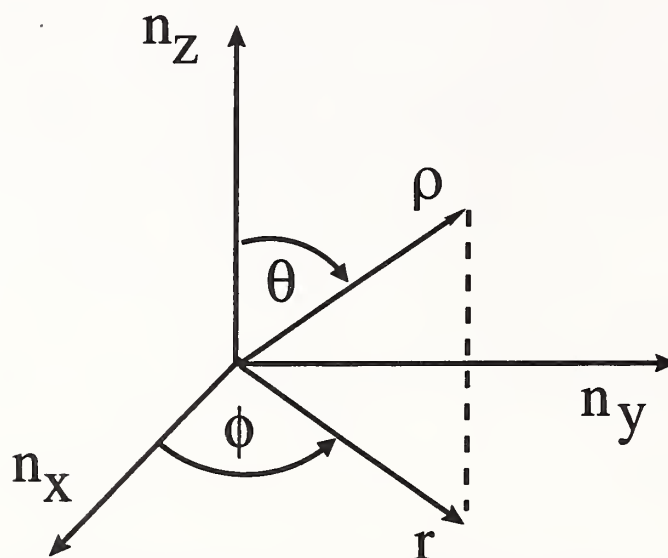


Figure 2. Schematic diagram of the spherical coordinate system (ρ, θ, ϕ) used for the definition of the surface energy $\gamma(\phi, \theta)$.



Figure 3. 3-D equilibrium shapes for $\epsilon_4 = -1/18$ (left) and $\epsilon_4 = 1/12$ (right).

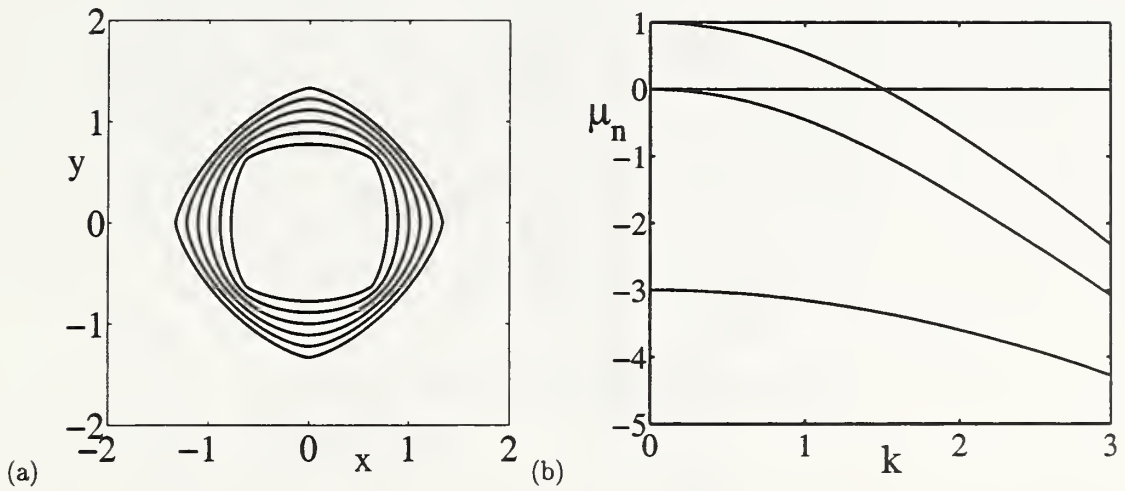


Figure 4. (a) Cross sections of the unperturbed rod for the [001] case: from the inner to the outer curve, $\epsilon_4 = -0.0556, -0.0278, 0, 0.0278, 0.0556,$ and 0.0833 . (b) The first three eigenvalues μ_n versus the wavenumber k for the [001] case with $\epsilon_4 = 1/12$.

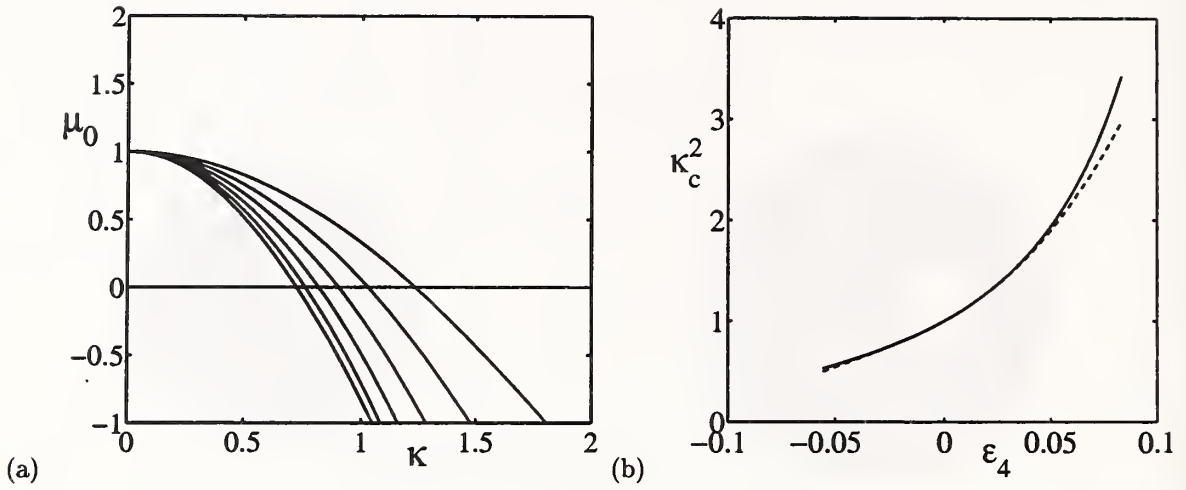


Figure 5. (a) Eigenvalues for $n = 0$ versus the rescaled wavenumber $\kappa = R_\epsilon k$ for the [001] case: from left to right, $\epsilon_4 = -0.0556, -0.0278, 0, 0.0278, 0.0556$, and 0.0833 . (b) The solid curve represents the square of the value of the rescaled critical wavenumber, κ_c^2 , versus ϵ_4 for the [001] case. The dashed curve shows the corresponding result from the asymptotic expansion for small ϵ_4 .

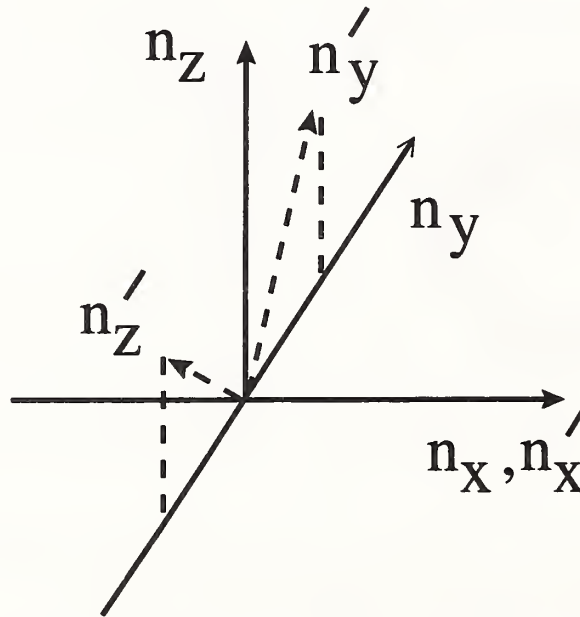


Figure 6. The orientation of the crystal axes (n'_x, n'_y, n'_z) relative to the coordinate system of the rod for the [011] case.

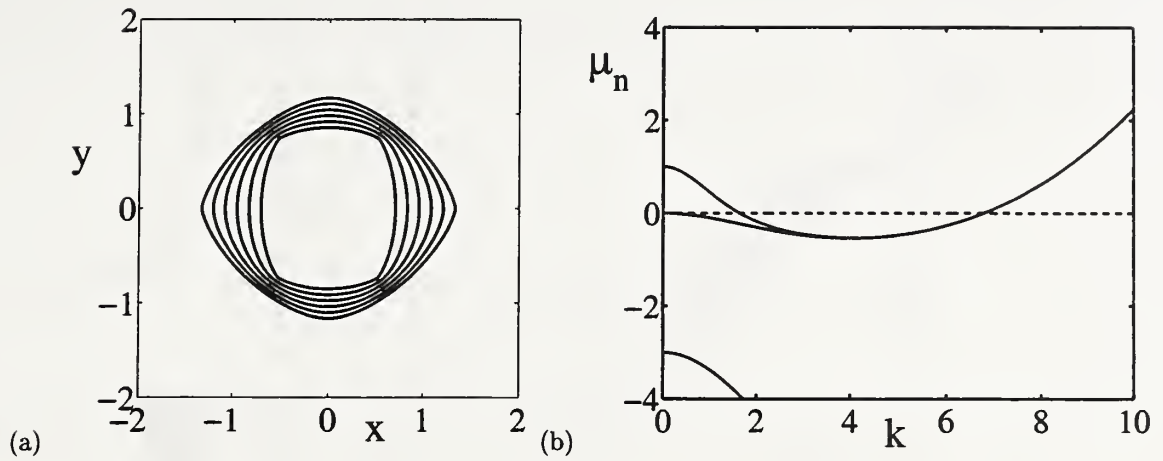


Figure 7. (a) Cross sections of the unperturbed rod for the [011] case: from the inner to the outer curve, $\epsilon_4 = -0.0735, -0.0422, -0.0108, 0.0206, 0.0520,$ and 0.0833 . (b) The first three eigenvalues versus the wavenumber k for the [011] case with $\epsilon_4 = -0.06$.

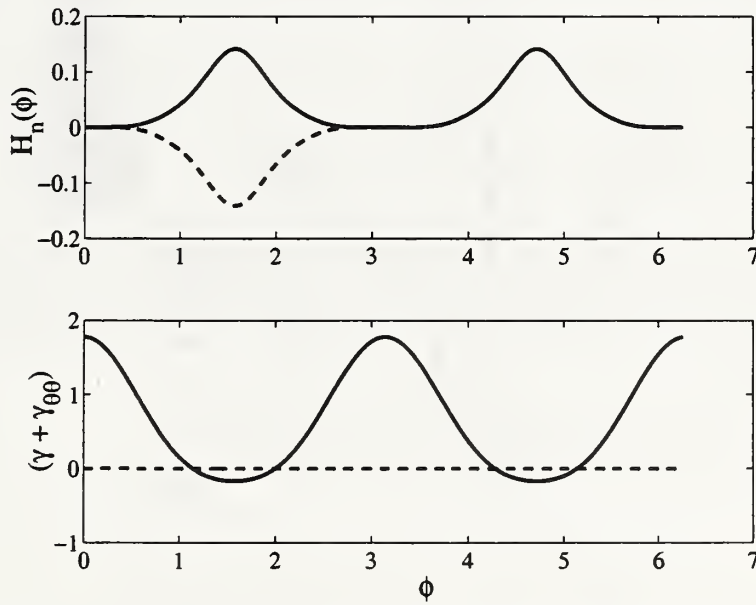


Figure 8. Top: the first (solid curve) and second (dashed curve) eigenmodes $H_n(\phi)$ for the [011] case with $k = 10$ and $\epsilon_4 = -0.06$. Bottom: the function $\gamma + \gamma_{\theta\theta}$ for $\epsilon_4 = -0.06$, exhibiting negative values near $\phi = \pi/2$ and $\phi = 3\pi/2$.

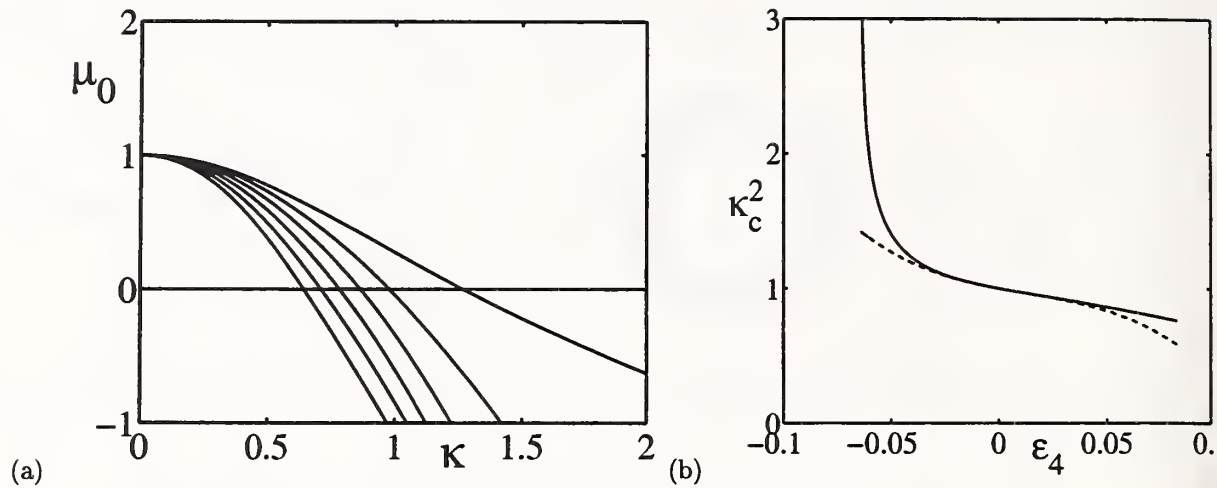


Figure 9. (a) Eigenvalues for $n = 0$ versus the rescaled wavenumber $\kappa = R_\epsilon k$ for the [011] case: from right to left, $\epsilon_4 = -0.0556, -0.0278, 0, 0.0278, 0.0556$, and 0.0833 . (b) The solid curve represents the square of the critical wavenumber, κ_c^2 , versus ϵ_4 for the [011] case. The large-wavenumber branch has a vertical asymptote at $\epsilon_4 = -1/18 \approx -0.0556$. The dashed curve shows the corresponding result from the asymptotic expansion for small ϵ_4 .

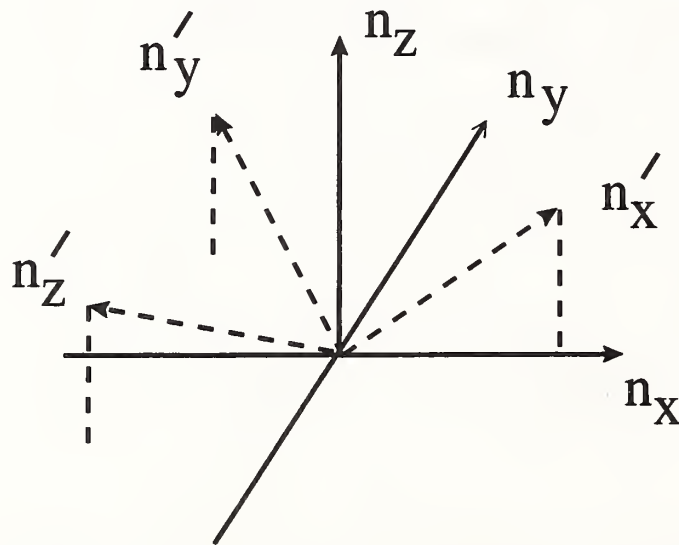


Figure 10. The orientation of the crystal axes (n'_x, n'_y, n'_z) relative to the coordinate system of the rod for the [111] case.

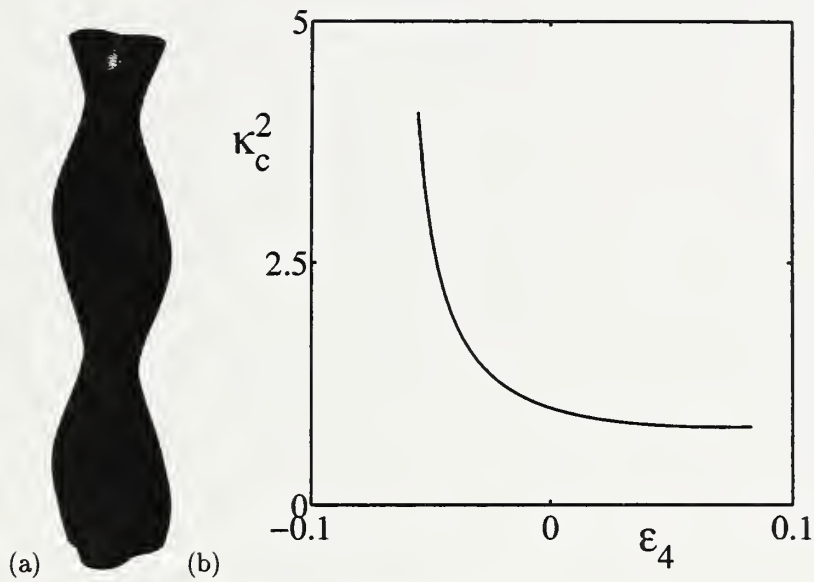


Figure 11. (a) Schematic illustration of the perturbed cylinder for the [111] case. Two wavelengths of a perturbation with $k = 1$ are shown. (b) The square of the value of the rescaled critical wavenumber, κ_c^2 , versus ϵ_4 for the [111] case. The corresponding result from the asymptotic expansion for small ϵ_4 is indistinguishable from the solid curve.

